RSC Advances

PAPER

View Article Online
View Journal | View Issue

Cite this: *RSC Adv.*, 2016, **6**, 28406

Mycobacterium tuberculosis histidinol dehydrogenase: biochemical characterization and inhibition studies†

Juleane Lunardi,[abc] Leonardo Kras Borges Martinelli,[a] Alessandra Silva Raupp,[a] José Eduardo Sacconi Nunes,[c] Diana Carolina Rostirolla,[a] Luís Fernando Saraiva Macedo Timmers,[d] Anne Drumond Villela,[a] Kenia Pissinate,[a] Jones Limberger,[a] Osmar Norberto de Souza,[abd] Luiz Augusto Basso,[abc] Diógenes Santiago Santos*[abc] and Pablo Machado*[ab]

Received 1st February 2016
Accepted 10th March 2016

DOI: 10.1039/c6ra03020c

www.rsc.org/advances

HisD-Encoded histidinol dehydrogenase (HisD) catalyzes the two last chemical reactions of the L-histidine biosynthetic pathway, namely the conversion of L-histidinol (L-Hol) to L-histidinaldehyde (L-Hal) and to L-histidine (L-His). The *hisD* gene product has been shown to be essential for *Mycobacterium tuberculosis* survival *in vitro*. Herein, we describe a series of biochemical studies on recombinant *Mycobacterium tuberculosis* HisD (*Mt*HisD). The synthesis of hydrazones derived from L-histidine yielded inhibitors in the low micromolar range, one of which showed moderate anti-Mtb activity. The compounds described here are, to the best of our knowledge, the first inhibitors of *Mt*HisD activity reported in the literature, and they could become promising candidates for future development.

Introduction

Tuberculosis (TB) continues to claim thousands of lives annually. According to the World Health Organization (WHO), 9.6 million new cases of the disease were reported worldwide in 2014 with 1.5 million deaths.[1] The elevated adaptive capacity of *Mycobacterium tuberculosis* (Mtb), the main etiological agent of human TB, and inappropriate treatments have fuelled the emergence of multi-drug-resistant (MDR-TB) and extensively drug-resistant (XDR-TB) strains for which available treatments are suboptimal and limited. Moreover, eradication of TB is hampered by asymptomatic infection from dormant or latent forms of mycobacteria, which have placed one-third of the world's population at lifelong risk for TB development from disease reactivation. To achieve infection control, there is an urgent need to develop drugs with novel mechanisms of action. Since the early 1960s, bedaquiline has been the sole drug presenting a new molecular target licensed for TB treatment. This ATP synthase targeted drug was approved for the treatment of adults with MDR-TB when other therapeutic alternatives are not available.[2–4] Although treatment with bedaquiline has been described as a promising strategy against MDR-TB strains, its possible cardiac safety concerns[5] and the rapid emergence of new drug-resistant strains have emphasized the need for continuing efforts to discover new TB drugs.

Within this context, the enzymes of the biosynthetic L-histidine pathway have emerged as attractive targets for the design and development of novel lead compounds, which can hopefully become innovative anti-mycobacterial drugs.[6] This pathway utilizes ten enzymatic reaction steps to convert phosphoribosyl pyrophosphate (PRPP) and ATP to L-histidine. Unlike mammals, the L-histidine pathway is present in prokaryotic organisms, lower eukaryotic organisms, and plants.[7–9] Consequently, the L-histidine pathway enzymes have been described as potential targets for the development of new herbicides and antimicrobial compounds endowed with selective toxicity.[10,11] It is important to note that this route shows connections to other biosynthetic pathways such as purine and tryptophan biosynthesis,[6,8,12] making it an important biochemical hub. The bifunctional histidinol dehydrogenase (EC 1.1.1.23), encoded by the *hisD* gene, is responsible for the two last reactions of this pathway, the NAD^+- and Zn^+-dependent conversion of L-histidinol (L-Hol) to L-histidine (L-His) through an L-histidinaldehyde (L-Hal) intermediate,[13–15] leading to the concomitant reduction of 2 NAD^+ molecules. The importance of L-histidinol

[a]*Instituto Nacional de Ciência e Tecnologia em Tuberculose (INCT-TB), Centro de Pesquisas em Biologia Molecular e Funcional, Pontifícia Universidade Católica do Rio Grande do Sul, 90619-900, Porto Alegre, RS, Brazil. E-mail: diogenes@pucrs.br; pablo.machado@pucrs.br; Fax: +55 51 33203629; Tel: +55 51 33203629*

[b]*Programa de Pós-graduação em Biologia Celular e Molecular, Pontifícia Universidade Católica do Rio Grande do Sul, 90619-900, Porto Alegre, Rio Grande do Sul, Brazil*

[c]*Quatro G Pesquisa & Desenvolvimento Ltda., 90619-900, Porto Alegre, Rio Grande do Sul, Brazil*

[d]*Laboratório de Bioinformática, Modelagem e Simulação de Biossistemas (LABIO), Pontifícia Universidade Católica do Rio Grande do Sul, 90619-900, Porto Alegre, Rio Grande do Sul, Brazil*

† Electronic supplementary information (ESI) available. See DOI: 10.1039/c6ra03020c

dehydrogenase for virulence has been demonstrated in pathogenic bacteria such as *Brucella suis* (*B. suis*),[16] *Salmonella* typhimurium (*S. typhimurium*),[17] and *Burkholderia pseudomallei* (*B. pseudomallei*).[18]

In Mtb, the enzyme histidinol dehydrogenase (*Mt*HisD) has been reported to be essential for survival and mycobacterial virulence.[19–22] Indeed, there is an apparent inability of histidine auxotrophs of Mtb to survive single-amino acid starvation under standard culture conditions,[19] and the *hisD* gene has been described as essential for *in vitro* mycobacterial growth.[20,22] Incidentally, *Mt*HisD has been classified among the top 50 targets by the TDR Targets Database.[21] This rank takes into account aspects such as the existence of a solved structure or structure model, essentiality in any species, the absence of a human ortholog, and expression during latency or dormancy. Accordingly, we have previously reported kinetic, thermodynamic and structural analyses of *Mt*HisD to aid the medicinal chemistry campaigns based on the rational drug design.[23] We have proposed that *Mt*HisD follows a Bi Uni Uni Bi Ping-Pong mechanism in which L-Hol is the first substrate to bind and that L-His is the last product to dissociate and that the amino-acid side chains of His336 and Glu335 are likely involved in catalysis and/or substrate binding.[23] Accordingly, imidazole-containing substrate analogues are likely to bind to free enzyme.

Our initial purpose was to try and maintain the possible polar non-covalent interaction mediated by the imidazole ring of L-Hol with catalytic amino acid residue His336 by synthesizing molecules with structural characteristics obtained from the substrate (L-Hol), intermediate (L-Hal), and product (L-His) of the enzyme-catalyzed chemical reaction. In addition, the designed compounds could explore the hydrophobic pocket near the NAD^+ in the catalytic site of *Mt*HisD in accordance with previously published data from orthologous enzymes.[24]

As an improved understanding of the mode of action of *Mt*HisD could help further medicinal chemistry efforts, here we present pre-steady kinetics studies, the activation energy of the catalyzed reaction, solvent kinetic isotope effects, proton inventory, and molecular crowding effects. Data on synthesis of hydrazones using L-histidine as a scaffold and their evaluation as *Mt*HisD enzyme inhibitors were described. In addition, docking experiments were performed to provide a three-dimensional picture of the interaction mode of selected inhibitors. The inhibitory activity on the growth of Mtb (minimum inhibitory concentration (MIC)) was also evaluated.

Experimental

All reagents for enzyme activity measurements and inhibition assays were purchased from Sigma-Aldrich and were used without further purification. All measurements were performed at least in duplicate, and the biochemical data, when necessary, were analyzed using the program SigmaPlot 10.0 (Systat Software, Inc.).

Enzyme assays

Cloning and overexpression of the *hisD*-encoding gene from *Mycobacterium tuberculosis*, purification, and determination of the true steady-state kinetic constants were performed as previously described.[23]

The reaction mixture used to determine the steady-state kinetic parameters for the histidinol substrate consisted of variable concentrations of L-Hol (2–120 μM) and a fixed-saturating concentration of NAD^+ (2×10^5 μM). For the NAD^+ substrate, variable concentrations of NAD^+ (700–20 000 μM) and a fixed-saturating concentration of L-Hol (200 μM) were used. Both assays were performed using 50 mM PIPES as buffer, pH 7.2 (0.5 mL final volume) at 25 °C, and the change in absorbance at 340 nm was monitored using a spectrophotometer (UV-2550 UV/visible, Shimadzu). One unit of enzyme activity (U) is defined as the amount of enzyme catalyzing the conversion of 1 μmol of substrate per minute in an optical path of 1 cm. The Michaelis–Menten constant (K_M) and k_{cat} values were calculated from eqn (1) and (2),[25] respectively:

$$v = \frac{V_{max}\,[S]}{K_M + [S]} \quad (1)$$

$$k_{cat} = \frac{V_{max}}{[E]_t} \quad (2)$$

where v is the steady-state velocity, V_{max} is the maximal rate, [S] is the substrate concentration, K_M is the Michaelis constant, k_{cat} is the catalytic constant, and $[E]_t$ is total concentration of enzyme.

Pre-steady-state kinetics

The increase in absorbance at 340 nm was monitored at 25 °C using an SX-18MV-R stopped-flow spectrofluorimeter (Applied Photophysics). The mixing chamber concentrations of enzyme and reagents in 50 mM PIPES pH 7.2 buffer were: *Mt*HisD at 10 μM, NAD^+ at 5×10^4 μM, and L-Hol at 1000 μM. The reaction time was 100 s. These measurements were performed to determine whether product release is part of the rate-limiting step. The control experiment was performed under the same conditions, but in the absence of enzyme. The data were fitted to eqn (3).

$$A = A_0\, e^{-kt} \quad (3)$$

where A is the absorbance at time t, A_0 is the absorbance at time zero, and k is the apparent first-order rate constant for product formation.

Energy of activation (E_a)

To determine the energy of activation of the *Mt*HisD-catalyzed chemical reaction, initial velocities were measured in the presence of saturating concentrations of both substrates (L-Hol 200 μM; NAD^+ 2×10^5 μM), at temperatures varying from 15 to 40 °C. The enzyme was incubated for three minutes at all temperatures tested and assayed under standard conditions. The E_a was calculated from the slope (E_a/R) of the Arrhenius plot fitting the data to eqn (4). With this result, we can estimate the thermodynamic activation parameters, such as the enthalpy ($\Delta H^{\#}$), free Gibbs energy ($\Delta G^{\#}$) and entropy ($\Delta S^{\#}$), from the transition state theory[26] (eqn (5)–(7)), respectively.

$$\ln k_{cat} = \ln A - \left(\frac{E_a}{R}\right)\frac{1}{T} \quad (4)$$

$$\Delta H^{\#} = E_a - RT \quad (5)$$

$$\Delta G^{\#} = RT\left(\ln\frac{k_B}{h} + \ln T - \ln k_{cat}\right) \quad (6)$$

$$\Delta S^{\#} = \frac{\Delta H^{\#} - \Delta G^{\#}}{T} \quad (7)$$

where R is the universal gas constant (8.314 J mol^{-1} K^{-1}), A is the Arrhenius constant, which represents the product of the collision frequency (Z) and a steric factor (p) based on the collision theory of enzyme kinetics,[26] T is the temperature in Kelvin ($T = °C + 273.15$), k_B is the Boltzmann constant (1.3805×10^{-23} J K^{-1}), and h is Planck's constant (6.6256×10^{-34} J s^{-1}). The error in $\Delta G^{\#}$ was calculated using eqn (8).

$$(\Delta G)_{Err} = \frac{RT(k_{cat})_{Err}}{k_{cat}} \quad (8)$$

Solvent kinetic isotope effects (SKIE) and proton inventory

Solvent kinetic isotope effects were determined by measuring initial velocity in the presence of varying concentrations of one of the substrates (L-Hol 4–200 μM or NAD^+ 100–20 000 μM) and a fixed-saturating concentration of the other substrate (L-Hol 200 μM or NAD^+ 2×10^5 μM). Both reactions were carried out in H_2O and in 90 atom% D_2O. Furthermore, the reactions were performed in 50 mM PIPES, pH 7.2, and in 50 mM Tris–HCl, pH 9.0 and enzyme velocity measurements were carried out at 25 °C. The data were fitted to eqn (9). The proton inventory was determined at 25 °C using saturating concentrations of both substrates (L-Hol 200 μM and NAD^+ 2×10^5 μM) at different mole fractions of D_2O (0–90%) in 50 mM PIPES, pH 7.2, or 50 mM Tris–HCl (pH 9.0). The solvent kinetic isotope effect data were fitted to eqn (9);[27] in which V is the maximal velocity, A is the substrate concentration, K is the Michaelis constant for A, $E_{V/K}$ and E_V are the isotope effects −1 on V/K and V, respectively, and F_i is the fraction of deuterium label in the substrate.

$$v = \frac{VA}{K(1 + F_i E_{V/K}) + A(1 + F_i E_V)} \quad (9)$$

The dome-shaped proton inventory data (Fig. 4) at pH 7.2 were fitted to eqn (10), and the linear data (Fig. 4 – inset) at pH 9.0 were fitted to eqn (11),[27] in which ${}^{n}k$ is equal to the ratio k_n/k_1 and ${}^{D_2O}k$ is equal to the ratio k_0/k_1, thus k_n is the k_{cat} at each atom% D_2O, k_0 is the k_{cat} with H_2O, n is the atom% D_2O, ϕ^T and ϕ^R represent transition state and reactant state fractionation factors, respectively. The superscripts T_1 and T_2 represent two different transition states in the reaction mechanism of *Mt*HisD that contribute to solvent isotope effects.

$${}^{n}k = {}^{D_2O}k\,\frac{\left(1 - n + n\phi^{T_1}\right)\left(1 - n + n\phi^{T_2}\right)}{1 - n + n\phi^{R}} \quad (10)$$

$${}^{n}k = {}^{D_2O}k(1 - n + n\phi^{T}) \quad (11)$$

Molecular crowding

The enzyme assay for L-Hol was carried out by varying the concentration of L-Hol (2–120 μM) and using a fixed-saturating concentration of NAD^+ (2×10^5 μM). For NAD^+, we used varying concentrations of NAD^+ (700–20 000 μM) and a fixed-saturating concentration of L-Hol (120 μM). The reactions were all performed at 25 °C in the absence or in the presence of 100 or 200 g L^{-1} of the inert polymer Ficoll PM70 (Sigma-Aldrich). The apparent parameters (K_M, k_{cat}, and specificity constant) were compared in the presence and absence of Ficoll.

Synthesis of hydrazone derivatives 4a–k

A simple three-step strategy was applied for the synthesis of histidinol dehydrogenase inhibitors. In the first step, L-histidine **1** was allowed to react with thionyl chloride in methanol, providing L-histidine methyl ester **2** with 96% yield (Scheme 1). Ester **2** was then reacted with hydrazine hydrate in methanol reflux, leading to hydrazide **3** with 80% yield.[28] It is noteworthy that the role of $NH_2NH_2 \cdot H_2O$ in this step is both to react with the ester moiety and to neutralize the medium, affording a nucleophilic unprotonated hydrazide. Another aspect that deserves to be mentioned is the labored separation of **3** from excess hydrazine hydrate impurities because this nucleophile was used in a 2.1 : 1 molar ratio in relation to L-histidine methyl ester **2**. To accomplish this task, we developed an alternative strategy: to react the crude product with 4-fluorobenzaldeyde in ethanol. In this way, the unwanted 4-(fluorobenzylidene) hydrazine precipitated, and pure **3** was obtained as a pale yellow oil.

With the precursor **3** in hand, it was reacted with a number of aldehydes, providing the products **4a–k** with yields ranging from moderate to good (Scheme 1). All synthesized compounds showed spectroscopic and spectrometric data in accordance with the proposed structures (ESI†).

Inhibition studies

Measurements of enzyme activity for inhibition studies were all carried out at 25 °C. The presence of time-dependent inhibitory activity was examined for the compounds synthesized. For this analysis, 1.5 μM of recombinant *Mt*HisD was pre-incubated with 2 μM of inhibitor. Afterward, aliquots were removed at different times (up to 30 min) and added to the reaction mixture (L-Hol, NAD^+, 50 mM PIPES pH 7.2 and H_2O, and final concentration of 3% DMSO). The change in initial *versus* time was monitored, and the percentage of inhibition was calculated.

To perform IC_{50} determinations, the compounds (dissolved in DMSO) were added at various concentrations, ranging from 0–120 μM, to the reaction mixture containing *Mt*HisD. The concentration of the added substrates (L-Hol and NAD^+) was fixed in K_M values[23] in the presence of 3% DMSO (a concentration that did not interfere with the assay conditions). The

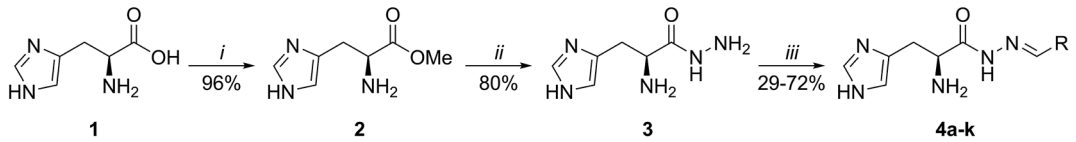

Comp.	R	Yield (%)
4a	Ph	40
4b	CH_3-4-C_6H_4	63
4c	Me_2N-4-C_6H_4	61
4d	MeO-4-C_6H_4	65
4e	Ph-4-O-Benzyl	72
4f	HO-2-C_6H_4	32
4g	F-4-C_6H_4	50
4h	Cl-4-C_6H_4	29
4i	Br-4-C_6H_4	60
4j	O_2N-4-C_6H_4	69
4k	2-Naphtyl	34

Scheme 1 Reactants and conditions: (i) = $SOCl_2$, MeOH, 65 °C, 16 h. (ii) = (1) $NH_2NH_2 \cdot H_2O$, MeOH, 65 °C, 16 h; (2), 4-fluorobenzaldehyde, EtOH, 25 °C, 1 h. (iii) = Benzaldehyde, EtOH, 79 °C, 4 h.

reactions were carried out at 25 °C in 50 mM PIPES pH 7.2 under standard conditions. The IC_{50} value, which defines the concentration of inhibitor required to reduce in 50% the initial enzyme activity, was determined by fitting the data to eqn (12).

$$\frac{v_i}{v_0} = \frac{1}{1 + \left(\frac{[I]}{IC_{50}}\right)^n} \quad (12)$$

in which v_i and v_0 are, respectively, the reaction velocity in the presence and in the absence of inhibitor (I).[29]

The inhibition constant (K_{is}) towards L-Hol was determined for compounds with IC_{50} values lower than 2.5 μM. The reaction mixture contained 0.36 μM of the enzyme, varying concentrations of L-Hol (2–120 μM), NAD^+ at the K_M concentration, and inhibitor at concentrations ranging from 0.5 to 30 μM. All enzyme velocity measurements were carried out at carried out at 25 °C. The K_{is} values were calculated from data fitting to competitive inhibition equation (eqn (13)), and the experimental data and predicted values were plotted as double-reciprocals as described by Lineweaver and Burk.[30]

$$v = \frac{V[S]}{K_M\left(1 + \frac{I}{K_{is}}\right) + [S]} \quad (13)$$

where V is the maximal velocity, K_M is the Michaelis–Menten constant, [S] is the substrate concentration, I is the inhibitor concentration, and K_{is} is the equilibrium dissociation constant for the enzyme–inhibitor complex.[31]

The equilibrium dissociation constant (K_d) for the lead-like compound **4k** was determined by fluorescence spectroscopy (Shimadzu RF-5301 PC spectrofluorophotometer). The excitation wavelength was 280 nm, and emission spectra were collected from 300 to 500 nm. The maximum value of fluorescence intensity at 334 nm was plotted as a function of increasing ligand concentration. The enzyme concentration was 2 μM (in 50 mM PIPES pH 7.2 buffer), and the compound concentration ranged from 0.499 to 4.93 μM. The enzyme and the compound were mixed and incubated for three minutes at assay temperature. Binary complex formation for each inhibitor concentration was measured by fluorescence titration, and the inner filter effect (50 mM PIPES buffer, pH 7.2, and varying concentration of the compounds, 0.499–4.93 μM) was subtracted. This experiment was performed at different temperatures (20, 25, and 30 °C). The dissociation constant values (K_d) were obtained from data fitting to eqn (14). The ln K_d values were plotted against the inverse of the temperature values, and the standard enthalpy of binding (ΔH°) and entropy of binding (ΔS°) were calculated from data fitting to the van't Hoff equation (eqn (15)). An estimate of the standard Gibbs free energy of binding (ΔG°) can thus be derived from eqn (16).

$$\frac{F_0 - F}{F_0 - F_\infty} = \frac{[L]}{K_d + [L]} \quad (14)$$

$$\ln K_d = \left(\frac{\Delta H^\circ}{R}\right)\frac{1}{T} - \frac{\Delta S^\circ}{R} \quad (15)$$

$$\Delta G^\circ = \Delta H^\circ - T\Delta S^\circ \quad (16)$$

F_0 represents the initial fluorescence, F is the observed fluorescence, F_∞ is the maximum change in fluorescence at saturating ligand (L) concentration, K_d represents the equilibrium dissociation constant for protein:ligand binary complex formation, R is the gas constant (8.314 J mol^{-1} K^{-1}), and T is the temperature in Kelvin.

Molecular docking experiments

These studies were performed to analyze the interaction mode of the selected compounds having K_{is} values for *Mt*HisD

inhibition lower than 5 μM. The enzyme and ligand structures were prepared using AutoDockTools 1.5.2, and docking simulations were performed with AutoDock 4.2, allowing flexibility in the ligands.[32,33] The experiments were performed with the homology model structure of *Mt*HisD associated with NAD^+.[23] Because the *Mt*HisD active site is at the interface of two subunits, we used the dimeric form to perform all docking experiments. For all simulations, the 3D-grid dimension used to define the enzyme active site and to evaluate the scoring function was 60 × 60 × 60, with spacing of 0.375 Å. The Lamarckian Genetic Algorithm (LGA) was employed as the docking algorithm with 50 runs, and the remaining parameters were set to their default values except for number of evaluations, which was set to 2 500 000.

Determination of minimum inhibitory concentration (MIC)

The growth inhibitory activity of the compounds was tested against the *Mycobacterium tuberculosis* H37Rv strain and was determined by resazurin microtiter assay (REMA).[34] Isoniazid was used as positive control. Mtb was cultivated in Middlebrook 7H9 (Difco) liquid medium supplemented with 10% (v/v) OADC (oleic acid, albumin, dextrose, catalase; Becton Dickinson), and 0.05% (m V^{-1}) Tween 80 (Sigma). Initially, it was grown at 37 °C up to an optical density at 600 nm (OD_{600}) between 0.6 and 0.8; then, it was diluted in Middlebrook 7H9 to an OD_{600} of 0.006. One hundred μL of Mtb inoculum were added to each well on a microplate containing 100 μL of the tested drug, or only Middlebrook 7H9 (control inoculum) to reach an OD_{600} of 0.003. Final drug concentrations ranged from 0.0078 to 4 μg mL^{-1} for isoniazid, and from 0.195 to 100 μg mL^{-1} for selected compounds. Plates were incubated for 7–9 days at 37 °C. Sixty microliters of 0.01% resazurin solution were added to each well; plates were re-incubated for additional 2 days. A change in color, from blue to pink, indicated the growth of bacteria, and the MIC was read as the minimum drug concentration that prevented the color change in resazurin solution. MIC values reported here represent an average of three tests carried out independently.

Results and discussion

*Mt*HisD is a bifunctional four-electron dehydrogenase enzyme that catalyzes two subsequent reactions, the oxidation of L-Hol and the reduction of two NAD^+ molecules,[23] with the formation of two intermediaries (L-Hal and L-histidindiol).[35] L-Hal is very unstable at neutral pH when not bound to HisD,[14,15,36,37] making study of the half-reaction difficult. The intermediates do not dissociate from the active site during the overall catalysis.[13] Another interesting aspect is that this enzyme has a single active site that carries out oxidations of both the L-Hol substrate and the L-Hal (aldehyde) intermediate.[13,14] These specific features reveal that the understanding of this enzymatic reaction is complicated, but very interesting in kinetic terms. A better understanding of the enzymatic mechanism's steps and the enzyme's interactions is important for the rational design of enzymatic inhibitors.

A pre-steady-state kinetics assay was performed to determine whether release of the product participates as a limiting step of the reaction. Fitting the data to eqn (3) resulted in an apparent first-order rate constant value of 0.0604 ± 0.0002 s^{-1} (Fig. 1), which describes a single exponential curve. As no burst in NADH formation could be detected (Fig. 1), this result suggests that product release does not contribute to the rate-limiting step of *Mt*HisD-catalyzed chemical reaction. Grubmeyer and

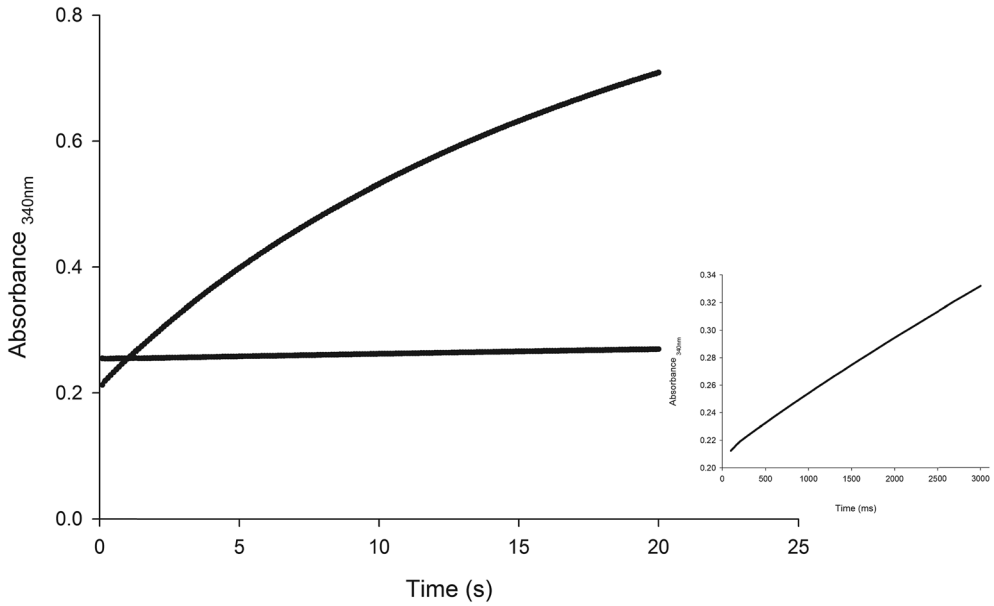

Fig. 1 Monophasic curve obtained in stopped-flow experiments, with single exponential enhancement in the absorbance at 340 nm upon conversion of NAD^+ to NADH catalyzed by 10 μM *Mt*HisD. The baseline represents the experimental control performed with 50 mM NAD^+ and 1 mM L-Hol in 50 mM PIPES pH 7.2 in the absence of recombinant *Mt*HisD enzyme. The inset highlights the curve at the time of 3 s.

Teng[38] showed that no burst could be detected for HisD from *Salmonella typhimurium* (*St*HisD). These authors concluded that the overall rates of the first and second half-reactions were not dramatically different, and thus both rates contribute to the overall rate limitation.

Experiments to determine the energy of activation of the rate-limiting step for the *Mt*HisD reaction were carried out. This energy represents the minimal amount of energy necessary to initiate the enzyme-catalyzed chemical reaction. The dependence of k_{cat} on temperature at saturating concentrations of L-Hol (200 μM) and NAD^+ (2×10^5 μM) was linear (Fig. 2). The linearity of the Arrhenius plot suggests that there is no change in the rate-limiting step over the temperature range utilized in the assay. These data were fitted to eqn (4), yielding a value of 45 (±2) kJ mol^{-1} K^{-1}, and the thermodynamic activation parameters were evaluated using eqn (5)–(7), yielding 42.25 (±0.04) kJ mol^{-1}; 72.07 (±0.07) kJ mol^{-1}; and −100 (±0.09) J mol^{-1} K^{-1} for $\Delta H^{\#}$, $\Delta G^{\#}$, and $\Delta S^{\#}$, respectively. The positive value (unfavorable) of $\Delta H^{\#}$ and the negative value (unfavorable) of $\Delta S^{\#}$ may be tentatively ascribed to loss of rotational and translational freedom, leading to a more positive value of $\Delta G^{\#}$. The positive value (unfavorable) of $\Delta G^{\#}$ represents the energy barrier to transforming ES in the ground state to the activated enzyme–substrate complex $ES^{\#}$.

The solvent kinetic isotope effects data (Fig. 3) were fitted to eqn (9), and the values obtained are presented in Table 1. The effect of D_2O on pH was recorded, and increasing in D_2O fractions, even after two minutes of enzyme addition, did not change the pH value. These results show contribution of proton transfer from the solvent to the *Mt*HisD-catalyzed chemical reaction. The fractionation factor (ϕ) is a measure of the stiffness or tightness of binding of a solute site *versus* the solvent sites. A general rule of thumb is that deuterium accumulates where binding is tighter ($\phi > 1$); and correspondingly, protium accumulates where binding is looser ($\phi < 1$).[27] The fractionation factors of transition state protons contribute reciprocally to the solvent kinetic isotope effect, whereas the contribution of a reactant state proton to the isotope effect is equal to its fractionation factor. The values of V and V/K in the assay at pH 7.2 (Table 1) suggest a modest participation of the proton solvent in catalysis and for L-Hol binding, whereas there appears to be no proton solvent isotope participation in NAD^+ binding (Fig. 3A and B). At pH 9.0, V and V/K showed normal solvent kinetic isotope effect for catalysis and inverse solvent isotope effect for L-Hol and NAD^+ binding (Fig. 3 – insets; Table 1). The reactant state for V/K is always free enzyme and free substrate and contribution of reactant state protons to solvent kinetic isotope effect is directly proportional to its fractionation factor. The reactant-state fractionation factors of functional groups that are involved in acid–base nucleophilic catalysis (*e.g.*, carboxylic group of glutamate, N–H bond of histidine, phenolic OH of tyrosine, *etc.*) are usually near unity.[27] It is thus tempting to suggest that at pH 9 there is an increase in the fractionation factor for transition state (deuterium accumulates in the transition state), whose reciprocal contribution results in an inverse V/K solvent kinetic isotope effect. Proton inventory experiments allow determination of the number of protons that are transferred during the solvent isotope-sensitive step, and can provide the basis for proposal of a model for the origins of solvent isotope effects on enzyme-catalyzed chemical reactions. The data at pH 7.2 showed a dome-shaped proton inventory (Fig. 4), which can have several mechanistic origins.[27] A tentative explanation may be that more than a single proton is transferred and that both normal and inverse solvent contributions were giving rise to the observed SKIE. Incidentally, Grubmeyer and Teng[38] reported a slightly convex downward curve in proton inventories, also suggesting the involvement of more than a single proton in the overall effect on *St*HisD. Fitting the data at pH 7.2 (Fig. 4) to eqn (10), in which the solvent isotope effect arises from a single offsetting reactant state (inverse SKIE) and two transition states (normal SKIE), appears to describe the experimental results. Although a crest-like curve in proton inventory could also be described by offsetting transition-state and medium contributions, the latter would require additional data to be invoked (*e.g.*, solute stability, equilibrium binding). At any rate, the data interpretation here presented is suboptimal, as the half reactions were not studied separately, and thus, these fractionation factors were not determined. The reaction mechanism for HisD from *Escherichia coli* (*E. coli*)[35] predicts at least two interactions between the transition states and the neighboring water molecule, which can influence SKIE. First, the water is activated by the negative charge of Glu326 (Glu335 in *Mt*HisD) and makes a nucleophilic attack on the carbonyl group of L-Hal, forming an L-histidindiol (gem-diol) intermediate. The unprotonated His327 of *E. coli* HisD (*Ec*HisD) (corresponding the conserved His336 in *Mt*HisD) abstracts a proton of the hydroxyl group bound to sp^3 carbon of L-histidindiol intermediate followed by hydride transfer to NAD^+ and formation of L-His. The protonated His327 of *Ec*HisD is restored to the neutral state by donation of a proton to the nearby water molecule.[35] This proposed mechanism suggests

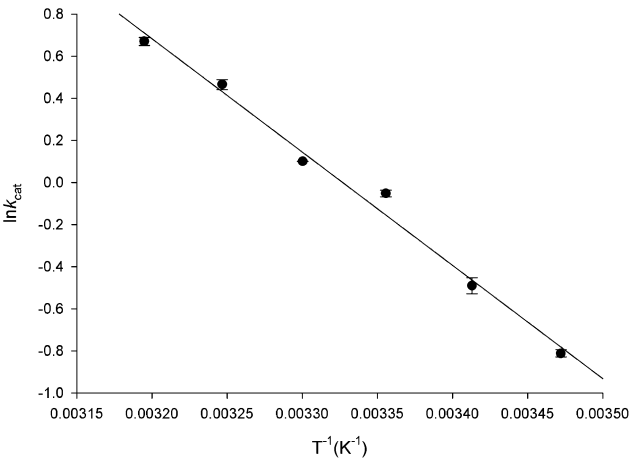

Fig. 2 Arrhenius plot for the temperature dependence of k_{cat}. Initial velocities were measured in the presence of saturating concentrations of L-Hol (200 μM) and NAD^+ (2×10^5 μM), at temperatures varying from 15 to 40 °C. The linearity of the maximum velocity *versus* temperature function suggests that there is no change in the rate-limiting step. The measurements are performed in duplicate and the data are expressed as the means ± SD.

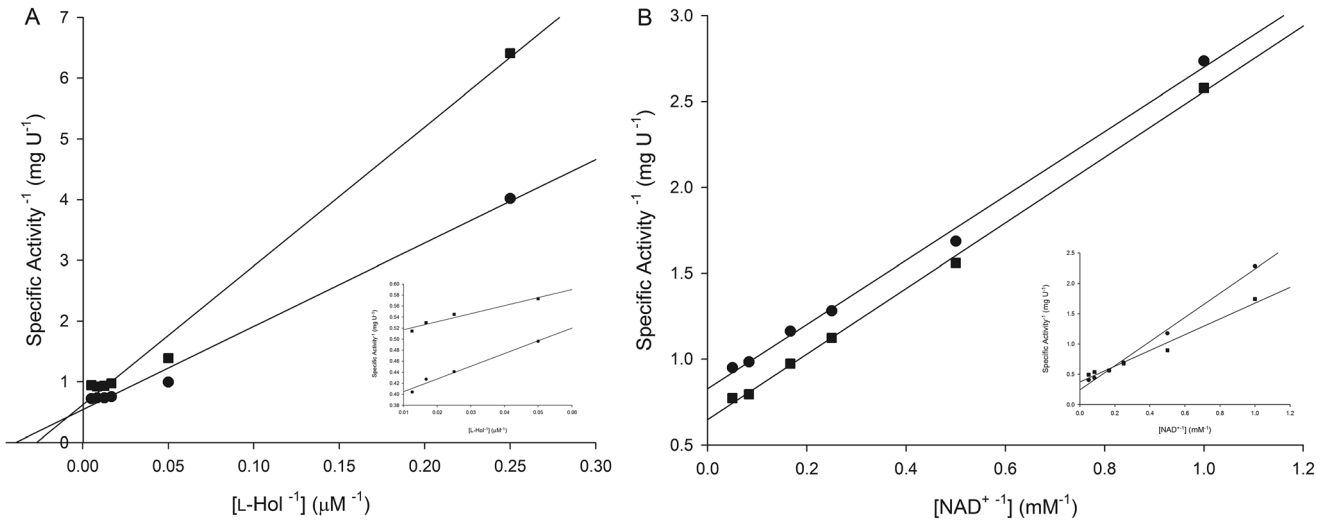

Fig. 3 Solvent kinetic isotope effects in (A) varying concentration of L-Hol (4–200 μM) and fixed-saturating concentration of NAD^+ (200 mM) at pH 7.2 (inset at pH 9.0), in (B) varying concentration of NAD^+ (1–20 mM) and fixed-saturating concentration of L-Hol (200 μM) at pH 7.2 (inset at pH 9.0). The lines represent fits to eqn (9). The values were obtained in either 0 (●) or 90 (■) atom% D_2O.

Table 1 Solvent kinetic isotope effects for *Mt*HisD

Parameters[a]	Isotope effect pH 7.2	Isotope effect pH 9.0
$V/K_{\text{L-Hol}}$	1.52 ± 0.32	0.61 ± 0.10
$V_{\text{L-Hol}}$	1.24 ± 0.06	1.39 ± 0.01
V/K_{NAD^+}	0.98 ± 0.04	0.60 ± 0.08
V_{NAD^+}	1.30 ± 0.02	1.44 ± 0.06

[a] V/K values are in U mg^{-1} μM^{-1}.

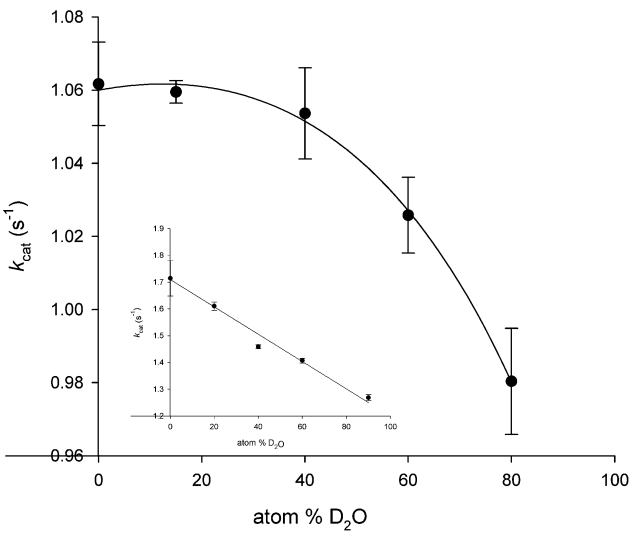

Fig. 4 Proton inventory using saturating concentrations of both substrates and variable atom% D_2O in 50 mM PIPES pH 7.2. The inset shows the proton inventory in 50 mM Tris–HCl pH 9.0. The determinations are carried out in duplicate and the data are expressed as the means ± SD.

that invoking two or more transition states to explain the proton inventory data here presented is warranted. However, additional studies are needed to clarify the exact fractionation factors that are influencing the SKIE. The proton inventory data at pH 9.0, on the other hand, suggest that a single transition-state proton transfer contributes to the solvent isotope effect (Fig. 4 – inset). Accordingly, the data were fitted to eqn (11). The proton inventory data at pH 9 are consistent with the normal solvent kinetic isotope effect for catalysis (Table 1).

It is known that the rate limiting chemical step can change as the pH changes, and the magnitude of the isotope effects on V and V/K change depending on the contribution of the isotope-sensitive step to overall rate limitation at saturating and limiting reactant concentrations, respectively.[39] According to the results here presented, the pH-dependent steps are isotope-sensitive. The difference of SKIE at two pHs can be related to the pK_a values of the residues involved in catalysis and L-Hol binding. The apparent pK value of L-Hol binding to free *Mt*HisD is approximately 8 ± 3 (the value attributed to conserved histidine residues in the active site).[23] Titration profiles for *St*HisD using L-Hol suggested an aminoacid side chain with pK values of 8.17 and 8.35 that are essential for, respectively, catalysis and L-Hol substrate binding.[38] It is likely that the imidazole side chain of His336 in *Mt*HisD is involved in coth L-Hol binding and catalytic activity of first and second hydride transfer in the reaction.[23] The differences in the results of the proton inventory, in the two tested pH, may be related to deprotonation of His336 at pH 9.0. As the physiological pH of the host is approximately 7.2, the results of SKIE and proton inventory at this pH reproduce with more reliability the environment found by Mtb when it infects a human cell. Following this line of reasoning, in an attempt to simulate the host cellular environment and to validate our results obtained in aqueous medium, crowding assays were performed.

Molecular crowding was carried out using an inert polymer to try to reproduce a cell-like environment with high concentrations of macromolecules. The values of steady-state kinetic parameters (K_M, k_{cat}, and specificity constant) in a solution containing Ficoll at two different concentrations in comparison to these parameters in the absence of Ficoll are presented in Table 2. These results validated our experiments with *Mt*HisD in aqueous solvent. Other works have obtained similar results. Molecular crowding experiments with phosphoglycerate kinase, glyceraldehyde-3-phosphate dehydrogenase, and acylphosphatase I enzymes in the presence of crowding agents also showed no influence of crowding agents on the kinetic parameters.[40]

Designed compounds **4** were synthesized in three steps with moderate to good yields (29–72%). The best yields were obtained for the reactions of 4-nitro-benzaldehyde (69%) and 4-benzyloxi-benzaldehyde (72%). However, 2-naphthaldehyde and 4-cholorobenzaldehyde converted to hydrazone derivatives with only 34% and 29% yield, respectively (for further information on synthesis of compounds, see the ESI†).

After obtaining the compounds, the next step was to evaluate them as possible inhibitors of the reaction catalyzed by *Mt*HisD. Inhibition studies of *S. typhimurium*,[41] cabbage, *E. coli*,[10] and *B. suis* HisD[24,28,42] have been reported in the literature.[6] In their first range of inhibitors, Abdo and colleagues[42] proposed benzylic ketones derived from L-His as inhibitors of *B. suis* HisD (*Bs*HisD) activity. In that report, an increased inhibition capacity of compounds with substitutions at the 4-position of the aromatic moiety was observed. The most effective compounds for inhibition of *Bs*HisD from the first library of compounds were 4-bromo and 4-benziloxy derivates.[42] A second series of L-histidinylphenylsulfonyl hydrazides[28] was less active than the one previously described, indicating that the nature and the length of the linker between the histidinyl moiety and the phenyl ring as well as the second lipophilic pocket binding the cofactor NAD^+ are important factors that can modulate the potency of new potential inhibitors.[24] It is important to emphasize that there is no report in the literature describing *Mt*HisD inhibition studies,[6] and the synthesized inhibitors compounds previously published for orthologous enzymes are chemically different from the synthesized compounds in this work. Abdo and colleagues studied the most promising series HisD inhibitors for *Bs*HisD,[24,42] but differences between the HisD of the *B. suis* and of the *M. tuberculosis* should be considered and these are showed in the Fig. 5.

Table 3 shows the IC_{50} values against *Mt*HisD activity for eleven compounds synthesized from L-histidine (Scheme 1) (for further information on IC_{50} measures, see the ESI†). No one of the ligands exhibited time-dependent inhibitory activity (data not shown). From these data, one can conclude that in general, compounds containing electron withdrawing groups at the 4-position of phenyl moieties demonstrated an increased inhibition capacity. Indeed, the 4-fluor-(**4g**), and 4-cloro-(**4h**), and 4-nitro-substituted compounds (**4j**) showed IC_{50} values of 2.4 ± 0.8 μM, 2.4 ± 0.4 μM, and 2.5 ± 0.2 μM, respectively. Polarization effects that modify the dipole vector of the compounds, facilitating van der Waals interactions, could thus rationalize these results. In accordance with previously reported data,[24,42] compounds with bulky substituents have shown better IC_{50} values for inhibiting HisD activity. The 2-naphthyl substituted compound **4k** was able to inhibit the catalytic activity of *Mt*HisD with an IC_{50} of 1.1 ± 0.2 μM. This planar π-electron rich group can make hydrophobic interactions with side chains of the amino acid residues of the active site of *Mt*HisD.

The K_{is} values (Table 4) were determined with respect to L-Hol substrate for four selected compounds (IC_{50} values lower than 2.5 μM, and molecule **4e**). Although hydrazone **4e** did not show an IC_{50} value lower than 2.5 μM (9.8 ± 0.7 μM), this compound was selected for additional inhibition studies because of its high lipophilicity. This characteristic is interesting for further MIC determination.

All tested molecules showed a competitive inhibition profile determined from the straight-line patterns intersecting at the *y*-axis (Fig. 6).[30] The competitive inhibition of the synthesized molecules, for L-Hol, corroborated the maintenance of chemical characteristics of substrate/product. These results evidence direct competition of the two ligands (substrate and inhibitor) for a common binding pocket on the enzyme molecule,[29] where the tested compounds bind to the free enzyme and exclude the substrate L-Hol binding. This mode of inhibition reduces the apparent affinity of the substrate by an amount that depends on the concentration and affinity of the inhibitor. Therefore, the substrate will bind to only the enzyme through the displacement of the inhibitor.[43]

To verify the choice of binding mode of hydrazones **4a–k** at the active site of *Mt*HisD, molecular docking simulations were carried out for selected compounds showing K_{is} values lower than 5 μM. The selected molecules showed interactions with amino acid residues involved in both catalysis and substrate binding. These experiments considered the amino acid residues

Table 2 Comparison of steady-state kinetics constants of *Mt*HisD in molecular crowding

Substrate	Ficoll (g L^{-1})	K_M (M)	k_{cat} (s^{-1})	k_{cat}/K_M[a] (M s^{-1})
L-Hol	—	20 (±5) × 10^{-6}	1.436 ± 0.001	7 (±2) × 10^4
	100	17 (±1) × 10^{-6}	1.209 ± 0.027	7.3 (±0.6) × 10^4
	200	22 (±5) × 10^{-6}	1.209 ± 0.083	6 (±1) × 10^4
NAD^+	—	2.9 (±0.1) × 10^{-3}	1.361 ± 0.038	4.7 (±0.2) × 10^2
	100	2.7 (±0.1) × 10^{-3}	1.134 ± 0.007	4.2 (±0.1) × 10^2
	200	3.3 (±0.4) × 10^{-3}	0.227 ± 0.015	69 (±10)

[a] Specificity constant.

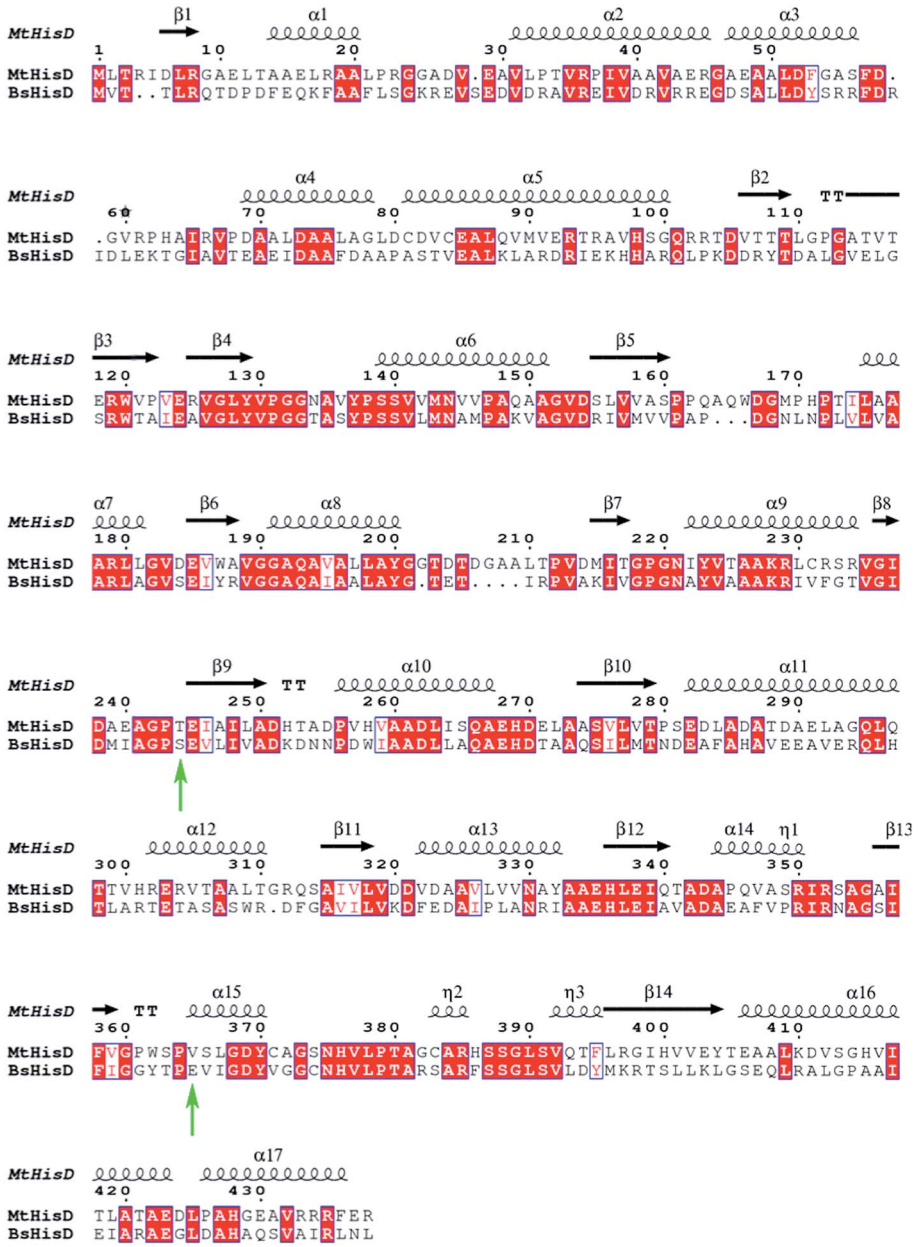

Fig. 5 Sequence alignment of *Mt*HisD and *Bs*HisD. The green arrows are highlighting the mutation encountered into the binding cavity. *M. tuberculosis* present a more hydrophobic binding site when compared to *B. suis,* since the physical–chemical properties of its residues (T244 and V357). The secondary structure was obtained based on the homology model of *Mt*HisD. All conserved residues are highlighted in red. Image generated with ESPript 3.0.[44]

involved in binding of L-Hol, NAD^+, and Zn^{2+} ion. These residues were determined in pH-rate profiles and molecular modeling experiments[23] based on the tridimensional structure of *Ec*HisD which was solved experimentally by X-ray diffraction at 1.7 Å resolution (PDB ID: 1KAE).[35] *Mt*HisD is a homodimeric enzyme, and its monomer (subunits A and B) possesses four globular domains.[23] The two active sites are located at the boundary of the homodimer interface. Domains 1, 2, and 4 are related to L-Hol and Zn^{2+} binding, and domain 1 to NAD^+ molecule binding.[23] Ligand **4e** was obtained to perform hydrophobic contacts with His376, which is involved in L-Hol binding (Fig. 7A), and Asp369. Therefore, the inhibitory capacity of compound **4e** could be a consequence of its large structure occupying the binding site of the L-Hol pocket, rather than of its binding potential to enzyme residues involved in L-Hol binding. Compounds **4h** and **4k** implement hydrophobic contacts with His336 (Fig. 7B and C), also involved in L-Hol binding. This amino acid residue acts as a base to abstract the proton from a hydroxyl group, causing the α-carbon to adopt a sp^2 configuration.[35] However, compound **4h** makes a hydrophobic interaction with Asp369, and the latter is involved in coordinating the Zn^{2+} ion (Fig. 7B). Considering that Zn^{2+} carries out an

Table 3 The IC_{50} values of the hydrazones derived from L-His

Comp.	R	IC_{50} (μM)
4a	Ph	29 ± 3
4b	CH_3-4-C_6H_4	5.5 ± 0.3
4c	Me_2N-4-C_6H_4	9.1 ± 0.3
4d	MeO-4-C_6H_4	5 ± 1
4e	Ph-4-O-benzyl	9.8 ± 0.7
4f	HO-2-C_6H_4	27 ± 2
4g	F-4-C_6H_4	2.4 ± 0.8
4h	Cl-4-C_6H_4	2.4 ± 0.4
4i	Br-4-C_6H_4	7.7 ± 0.7
4j	O_2N-4-C_6H_4	2.5 ± 0.2
4k	2-Naphtyl	1.1 ± 0.2

Table 4 Inhibition constants of select compounds

Comp.	K_{is} (μM)
4e	3.2 ± 0.6
4g	13 ± 2
4h	0.64 ± 0.07
4k	0.47 ± 0.06

important function in the correct positioning of L-Hol,[23,35] it is expected that those compounds acting as competitive inhibitors of L-Hol interact with the Zn^{2+}-binding amino acid residues. The **4k** molecule makes a hydrogen bond (H-bond) with $Asp369^{OD2}$ (Fig. 7C). The **4h** and **4k** candidates can have H-bond interactions with $His376^{ND1}$. The carbonyl backbones of this amino acid residue and of His336 are responsible for the formation of H-bonds with hydroxyl groups of the L-Hol substrate.[23] Participation of the Glu335 in either catalysis or substrate binding had not been demonstrated in pH-rate profile experiments with *Mt*HisD.[23] However, in *Ec*HisD-catalyzed reactions, Glu326 (corresponding to Glu335 in *Mt*HisD) activates the water molecule at the second step of the reaction.[35] The molecule **4h** interacts by H-bonding with $Glu335^{OE2}$, and this may interfere with activation of the water molecule and inhibit the nucleophilic attack on the reactive carbon for L-Hal. Compound **4k** can make H-bonding interactions with $Glu423^{OE1}$, which is related to L-Hol binding similarly to His336 and His376.[23] In addition, the hydrogen interactions of the N4 atom from **4k** imidazole portion with $His376^{ND1}$ were determined to be very important because this amino acid residue interacts directly with the

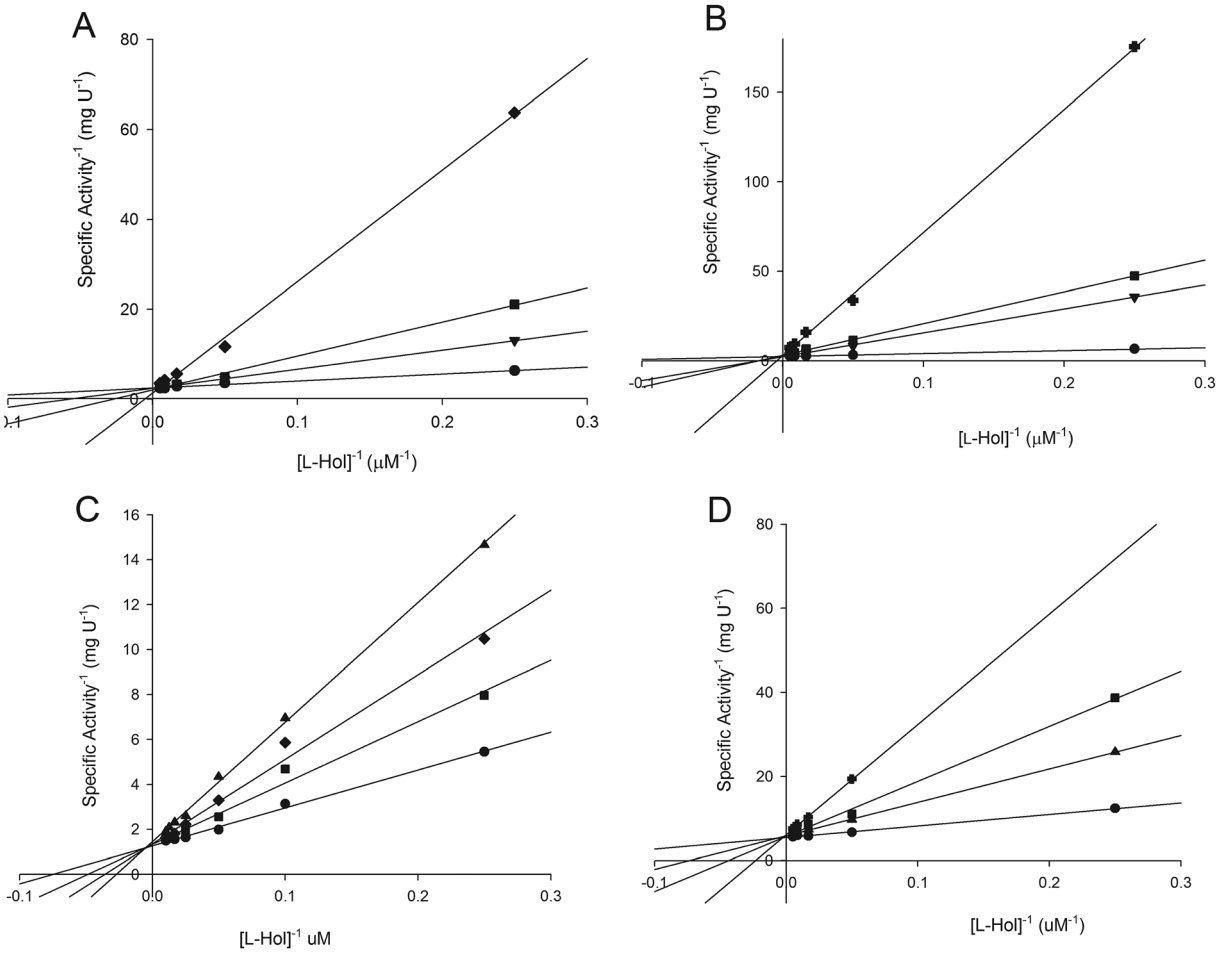

Fig. 6 Determination of inhibition mode for selected compounds. (A) Represents **4e**, (B) **4h**, (C) **4g**, and (D) **4k**. The Lineweaver–Burk plots display lines that intersect at the *y*-axis, which are diagnostic of competitive inhibition for all compounds tested. Thus, the V_{max} value is constant at all inhibitor concentrations, but the apparent value of K_M increases with increasing inhibitor concentration. Each line represents a different inhibitor concentration fitted to eqn (14) in a double reciprocal plot of *Mt*HisD specific activity by L-Hol substrate.

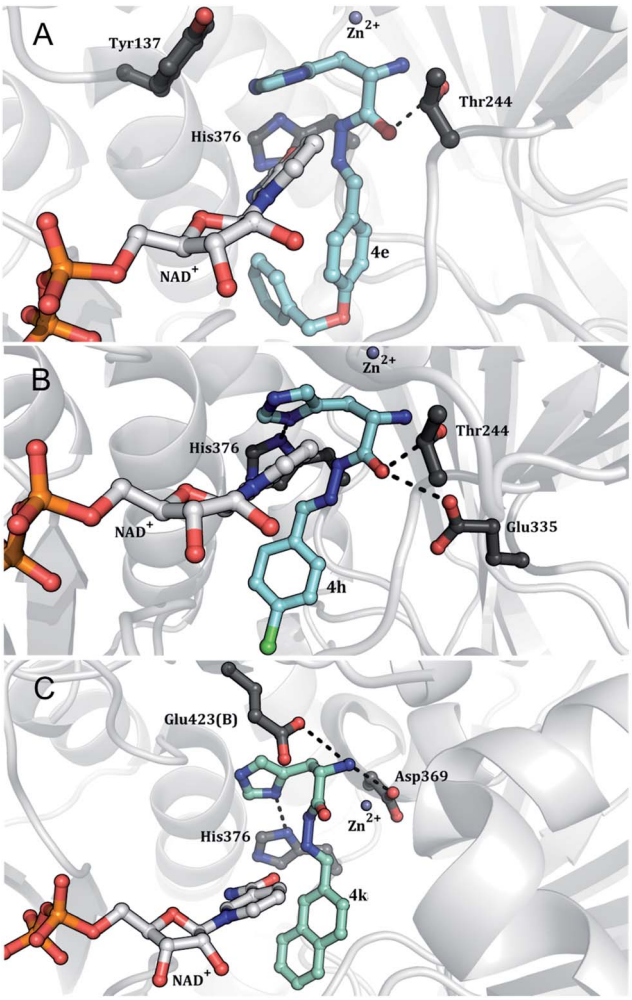

Fig. 7 Molecular docking results of *Mt*HisD. The best docking poses of the compounds **4e** (A), **4h** (B), and **4k** (C) into the *Mt*HisD binding cavity. *Mt*HisD tertiary structure is represented as cartoon colored in gray. The small molecules and the residues are represented as ball and stick models and colored in CPK, except the carbon atoms that are colored in black (residues), cyan (compounds), and gray (NAD^+). Image generated with PyMOL.[45]

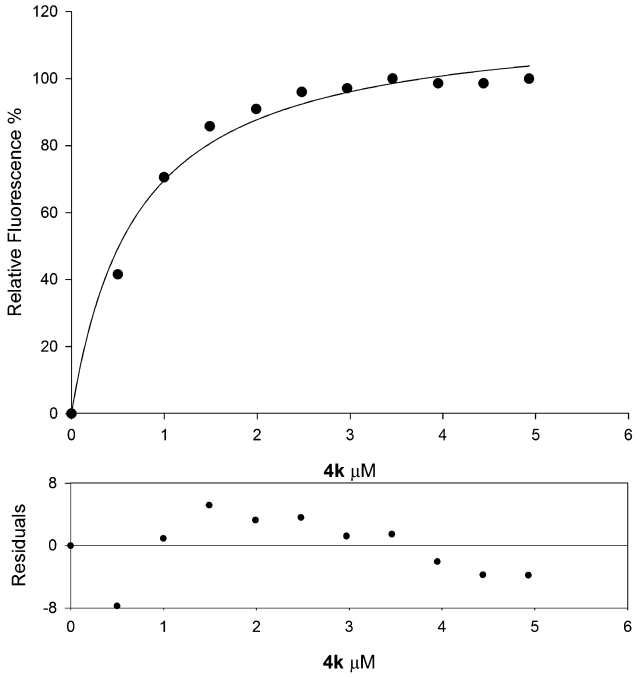

Fig. 8 Fluorescence spectroscopy of the equilibrium binding of compound **4k** to *Mt*HisD, plotting the relative fluorescence change as a function of **4k** concentration at 25 °C, and residuals.

hydroxyl group of L-Hol.[35] Finally, the number and relative force of the interactions performed by **4k** in molecular recognition can explain its higher inhibitory activity on *Mt*HisD. Equilibrium fluorescence spectroscopy data were fitted to eqn (14). As *Mt*HisD has four tryptophan amino acid residues and seven tyrosine residues, changes in protein Trp and Tyr fluorescence upon ligand binding were monitored. Titration of *Mt*HisD with the best ligand in inhibition assays (**4k**) showed a hyperbolic curve (Fig. 8), yielding K_d values of 0.62 ± 0.14 μM, 0.7 ± 0.1 μM, and 0.79 ± 0.15 μM, at 20 °C, 25 °C, and 30 °C, respectively. The K_d of **4k** binding to *Mt*HisD at 25 °C is in agreement with the K_{is} value of 0.47 μM for the same ligand. The K_d value of **4k** was lower than the K_d of 9 μM for L-Hol:*Mt*HisD binary complex formation obtained by ITC.[23]

The van't Hoff equation (eqn (15)) allowed determination of the individual contributions of ΔH° and $T\Delta S^\circ$ of the inhibitor's Gibbs free energy of binding from measurements of K_d as a function of temperature (Fig. 9).[29] The values obtained for ΔH° and ΔS° were -17.9 ± 0.2 kJ mol^{-1} (-4.28 ± 0.05 kcal mol^{-1}), and $5.77 \pm 0.052 \times 10^{-2}$ kJ mol^{-1} K^{-1} (1.3791 ± 0.0001 kcal mol^{-1} K^{-1}), respectively. The negative value (favorable) of ΔH° achieved for ligation of compound **4k** with free *Mt*HisD showed the release of heat, in contrast to *Mt*HisD:L-Hol ligation, which is unfavorable. In other words, it needs to absorb heat (positive value) to occur ($\Delta H^\circ = 3.6 \pm 0.5$ kcal mol^{-1} (ref. 23)). However, the positive ΔS° value (favorable) obtained was lower than the ΔS° of binding for *Mt*HisD:L-Hol binary complex formation (0.035 ± 0.013 kcal mol^{-1} K^{-1} (ref. 23)). Estimates for ΔG°

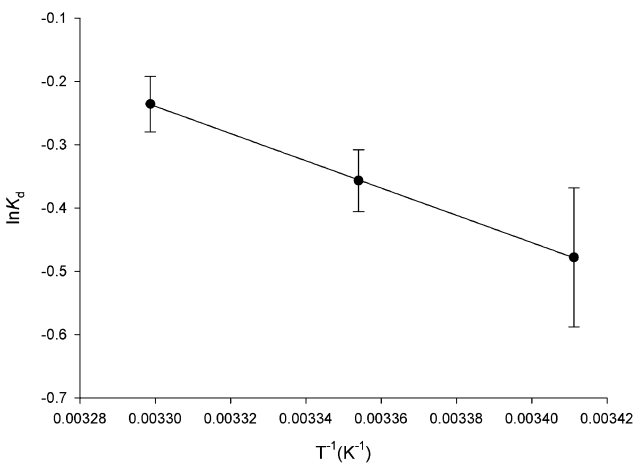

Fig. 9 Dissociation constant as a function of temperature. The curve was fitted using the van't Hoff equation (eqn (15)), and the ΔH°, and ΔS° terms could be estimated. Data are expressed as the means ± SD.

values were calculated employing eqn (16), yielding a value for ΔG° of -35.1 ± 4.9 kJ mol^{-1} (-8.39 ± 1.17 kcal mol^{-1}) in the temperature range of 20–30 °C. The favorable (negative) Gibbs free energy of binding demonstrates the spontaneous formation of the *Mt*HisD:**4k** complex. Compared to the *Mt*HisD:L-Hol binary complex ΔG° value of -7 ± 3 kcal mol^{-1},[23] binding of **4k** compound to free *Mt*HisD is more favorable than the L-Hol substrate binding. This result is in accordance with the competitive inhibition of the L-Hol profile by compound **4k**.

Finally, minimum inhibitory concentration is defined as the lowest drug concentration that prevents a color change in the REMA plate method.[34] Determination of MIC results for compound **4e** demonstrated that 100 μg mL^{-1} of the inhibitor molecule is needed to stop Mtb growth. In addition, compounds **4h** and **4k** showed MICs > 100 μg mL^{-1}. These results show that improvements in the molecule to increase its inhibitory potential and/or its ability to penetrate Mtb are necessary.

Conclusions

In summary, our results represent, in our opinion, an important advance in understanding the mechanism of the chemical reaction catalyzed by *Mt*HisD. In addition, to the best of our knowledge, hydrazones derived from L-histidine are the first low micromolar inhibitors of *Mt*HisD activity described in the literature. Moreover, these compounds presented moderate *in vitro* anti-Mtb activity against the *M. tuberculosis* H37Rv strain. Taken together, the results here presented are useful for the rational design of inhibitory molecules targeting *Mt*HisD activity, which hopefully could be further developed into novel alternative therapeutics against tuberculosis.

Conflict of interest

The authors declare no competing financial interest.

Authors contribution

The manuscript was written through contributions of all authors. All authors have given approval to the final version of the manuscript.

Acknowledgements

This work was supported by Quatro G P&D Ltda., and FAPERGS/SEBRAE (FAPERGS n. 013/2011). Financial support was also provided by National Institute of Science and Technology on Tuberculosis (Decit/SCTIE/MS-MCT-CNPq-FNDCT-CAPES), FAPERGS (ARD/2012), and CNPq (Process number 478959/2013-3). O.N.S. (CNPq, 305984/2012-8), L.A.B. (CNPq, 5201182/99-5), D.S.S. (CNPq, 304051/1975-06), and P.M. (CNPq, 307878/2015-5) are research career awardees of the National Council for Scientific and Technological Development of Brazil (CNPq). The fellowships from CNPq, CAPES, and FAPERGS are also acknowledged.

References

1 World Health Organization, *Global Tuberculosis Report 2015*, WHO Press, Geneva, 2015.
2 K. Andries, P. Verhasselt, J. Guillemont, H. W. H. Gohlmann, J.-M. Neefs, H. Winkler, J. van Gestel, P. Timmerman, M. Zhu, E. Lee, P. Williams, D. de Chaffoy, E. Huitric, S. Hoffner, E. Cambau, C. Truffot-Pernot, N. Lounis and V. Jarlier, *Science*, 2005, **307**, 223–227.
3 M. R. De Jonge, L. H. M. Koymans, J. E. G. Guillemont, A. Koul and K. Andries, *Proteins: Struct., Funct., Bioinf.*, 2007, **67**, 971–980.
4 A. H. Diacon, A. Pym, M. Grobusch, R. Patientia, R. Rustomjee, L. Page-Shipp, C. Pistorius, R. Krause, M. Bogoshi, G. Churchyard, A. Venter, J. Allen, J. C. Palomino, T. De Marez, R. P. G. van Heeswijk, N. Lounis, P. Meyvisch, J. Verbeeck, W. Parys, K. de Beule, K. Andries and D. F. Mc Neeley, *N. Engl. J. Med.*, 2009, **360**, 2397–2405.
5 J. Avorn, *JAMA, J. Am. Med. Assoc.*, 2013, **309**, 1349–1350.
6 J. Lunardi, J. E. S. Nunes, C. V. Bizarro, L. A. Basso, D. S. Santos and P. Machado, *Curr. Top. Med. Chem.*, 2013, **13**, 2866–2884.
7 B. N. Ames, B. Garry and L. A. Herzenberg, *J. Gen. Microbiol.*, 1960, **22**, 369–378.
8 P. Alifano, R. Fani, P. Liò, A. Lazcano, M. Bazzicalupo, M. S. Carlamagno and C. B. Bruni, *Microbiol. Rev.*, 1996, **60**, 44–69.
9 A. Stepansky and T. Leustek, *Amino Acids*, 2006, **30**, 127–142.
10 J. E. Dancer, M. J. Ford, K. Hamilton, M. Kilkelly, S. D. Lindell, M. J. O'Mahony and E. A. Saville-Stones, *Bioorg. Med. Chem. Lett.*, 1996, **6**, 2131–2136.
11 K. Gohda, D. Ohta, G. Iwasaki, P. Ertl and O. Jacob, *J. Chem. Inf. Comput. Sci.*, 2001, **41**, 196–201.
12 A. V. Due, J. Kuper, A. Geerlof, J. P. von Kries and M. Wilmanns, *Proc. Natl. Acad. Sci. U. S. A.*, 2011, **108**, 3554–3559.
13 E. Adams, *J. Biol. Chem.*, 1954, **209**, 829–846.
14 E. Adams, *J. Biol. Chem.*, 1955, **217**, 325–344.
15 J. C. Loper and E. Adams, *J. Biol. Chem.*, 1965, **240**, 788–795.
16 S. Kohler, V. Foulongne, S. Ouahrani-Bettache, G. Bourg, J. Teyssier, M. Ramuz and J. Liautard, *Proc. Natl. Acad. Sci. U. S. A.*, 2002, **99**, 15711–15716.
17 P. I. Fields, R. V. Swanson, C. G. Haidaris and F. Heffron, *Proc. Natl. Acad. Sci. U. S. A.*, 1986, **83**, 5189–5193.
18 S. Pilatz, K. Breitbach, N. Hein, B. Fehlhaber, J. Schulze, B. Brenneke, L. Eberl and I. Steinmetz, *Infect. Immun.*, 2006, **74**, 3576–3586.
19 T. Parish, *J. Bacteriol.*, 2003, **185**, 6702–6706.
20 C. M. Sassetti, D. H. Boyd and E. J. Rubin, *Mol. Microbiol.*, 2003, **48**, 77–84.
21 F. Aguero, B. Al-Lazikani, M. Aslett, M. Berriman, F. S. Buckner, R. K. Campbell, S. Carmona, I. M. Carruthers, A. W. E. Chan, F. Chen, G. J. Crowther, M. A. Doyle, C. Hertz-Fowler, A. L. Hopkins, G. McAllister, S. Nwaka, J. P. Overington, A. Pain, G. V. Paolini, U. Pieper,

S. A. Ralph, A. Riechers, D. S. Roos, A. Sali, D. Shanmugam, T. Suzuki, W. C. van Voorhis and C. L. M. J. Verlinde, *Nat. Rev. Drug Discovery*, 2008, **7**, 900–907.

22 M. A. DeJesus, Y. J. Zhang, C. M. Sassetti, E. J. Rubin, J. C. Sacchettini and T. R. Ioerger, *Bioinformatics*, 2013, **29**, 695–703.

23 J. E. S. Nunes, R. G. Ducati, A. Breda, L. A. Rosado, B. M. de Souza, M. S. Palma, D. S. Santos and L. A. Basso, *Arch. Biochem. Biophys.*, 2011, **512**, 143–153.

24 M.-R. Abdo, P. Joseph, J. Mortier, F. Turtaut, J.-L. Montero, B. Masereel, S. Kohler and J.-Y. Winum, *Org. Biomol. Chem.*, 2011, **9**, 3681–3690.

25 I. H. Segel, *Enzyme Kinetics – Behavior Analysis of Rapd Equilibrium and Steady-state Enzyme Systems*, Wiley, Classics Library Edition, Wiley- interscience, John Wiley & Sons, Inc., Hoboken, NJ, 1993.

26 T. Lonhienne, E. Baise, G. Feller, V. Bouriotis and C. Gerday, *Biochim. Biophys. Acta*, 2001, **1545**, 349–356.

27 P. F. Cook, *Enzyme Mechanism from Isotope Effects*, CRC Press, Boca Raton, 1991.

28 M.-R. Abdo, P. Joseph, R.-A. Boigegrain, J.-L. Montero, S. Kohler and J.-Y. Winum, *J. Enzyme Inhib. Med. Chem.*, 2008, **23**, 357–361.

29 R. A. Copeland, *Evaluation of Enzymes Inhibitors in Drug Discovery: A Guide for Medicinal Chemists and Pharmacologists*, Wiley-interscience, John Wiley & Sons, Inc., Hoboken, NJ, 1st edn, 2005.

30 H. Lineweaver and D. Burk, *J. Am. Chem. Soc.*, 1934, **56**, 658–666.

31 R. A. Copeland, *Enzymes: A Practical Introduction to Structure, Mechanism, and Data Analysis*, Wiley-interscience, John Wiley & Sons, Inc., Hoboken, NJ, 2nd edn, 2000.

32 G. M. Morris, R. Huey, W. Lindstrom, M. F. Sanner, R. K. Belew, D. S. Goodsell and A. J. Olson, *J. Comput. Chem.*, 2009, **30**, 2785–2791.

33 D. S. Goodsell and A. J. Olson, *Proteins: Struct., Funct., Bioinf.*, 1990, **8**, 195–202.

34 J.-C. Palomino, A. Martin, M. Camacho, H. Guerra, J. Swings and F. Portaels, *Antimicrob. Agents Chemother.*, 2002, **46**, 2720–2722.

35 J. A. R. G. Barbosa, J. Sivaraman, Y. Li, R. Larocque, A. Matte, J. D. Schrang and M. Cygler, *Proc. Natl. Acad. Sci. U. S. A.*, 2002, **99**, 1859–1864.

36 E. Adams, *J. Biol. Chem.*, 1955, **217**, 317–324.

37 H. Gorish and W. Holke, *Eur. J. Biochem.*, 1985, **150**, 305–308.

38 C. Grubmeyer and H. Teng, *Biochemistry*, 1999, **38**, 7355–7362.

39 P. F. Cook and W. W. Cleland, *Enzyme Kinetics and Mechanism*, Garland Science Publishing, NY, 2007.

40 T. Vopel and G. Makhatadze, *PLoS One*, 2012, **7**, e39418.

41 C. T. Grubmeyer, S. Insinga, M. Bhatia and N. Moazami, *Biochemistry*, 1989, **28**, 8174–8180.

42 M.-R. Abdo, P. Joseph, R.-A. Boigegrain, J.-P. Liautard, J.-L. Montero, S. Kohler and J.-Y. Winum, *Bioorg. Med. Chem.*, 2007, **15**, 4427–4433.

43 A. Schon, S. Y. Lam and E. Freire, *Future Med. Chem.*, 2011, **3**, 1129–1137.

44 X. Robert and P. Gouet, *Nucleic Acids Res.*, 2014, **42**(W1), W320–W324.

45 *The PyMOL molecular graphics system, version 1.3 r1*, L. L. C. SCHRODINGER, 2010.